ADVANCED ELECTRONIC MATERIALS
www.advelectronicmat.de

Semiconducting Copolymers Based on *meso*-Substituted BODIPY for Inverted Organic Solar Cells and Field-Effect Transistors

Mehmet Ozdemir, Sang Woo Kim, Hyungsug Kim, Myung-Gil Kim, Bumjoon J. Kim, Choongik Kim,* and Hakan Usta**

The synthesis, physicochemical, and optoelectronic properties of a new class of low band-gap (≈1.3 eV) donor–acceptor copolymers based on a highly electron-deficient *meso*-5-(2-octyldodecyl)thiophene-substituted BODIPY π-unit are presented. The polymeric solutions exhibit strong aggregation-dependent excitonic properties indicating the presence of enhanced π-coherence as a result of strong interchain interactions. The polymeric semiconductor thin films prepared by spin coating show isotropic nodule-like grains with essentially no ordering in the out-of-plane direction. Field-effect hole mobilities of 0.005 $cm^2 V^{-1}·s^{-1}$ are observed in bottom-gate top-contact organic field-effect transistors, and inverted bulk-heterojunction organic photovoltaics employing the polymer:$PC_{71}BM$ active layer exhibit excellent power conversion efficiencies of 6.2% with a short-circuit current of 16.6 mA cm^{-2}. As far as it is known, this is a record high value achieved to date for a boron-containing donor polymer in the photovoltaic literature indicating a significant enhancement in power conversion efficiency (>3–4 times). The findings clearly present that rationally designed BODIPY-based donor–acceptor copolymers can be a key player in photovoltaic applications.

1. Introduction

The novel solution-processable semiconducting polymers for organic optoelectronic technologies have developed rapidly within the recent decades, because of their emerging applications in new-generation flexible and roll-to-roll processed electronic devices such as organic field-effect transistors (OFETs) and bulk-heterojunction organic photovoltaics (BHJ-OPVs).[1–9] This progress is mainly driven by a combination of rational materials design and extensive exploratory synthesis.[10–15] In particular, donor–acceptor (D–A) conjugated polymers with alternating electron-rich (D) and electron-deficient (A) units offer the great advantage of fine-tuning optoelectronic/physicochemical properties.[12,16–20] This allows the realization of any desired copolymer property for a particular application by simply choosing the proper D–A units. Importantly, this strategy can yield low band-gap (<1.5 eV) copolymers with highly extended π-conjugations, providing access to a variety of state-of-the-art performances in polymer-based OFETs and OPVs. Specifically, the reported charge-carrier mobilities with D–A copolymers in OFETs are now routinely higher than that of amorphous silicon (>0.5–1.0 $cm^2 V^{-1}·s^{-1}$) and power conversion efficiencies (PCEs) of 10–12% are now available with D–A copolymer-based BHJ solar cells.[21–30] Despite these recent advances in polymer-based optoelectronics, there is still only a handful example of π-acceptor building blocks realized in the structure of D–A copolymers, which are mainly based on diketopyrrolopyrrole (DPP),[27,31,32] isoindigo,[33] benzo(bis)thiadiazole,[34] rylenediimide,[35–40] and thieno[3,4-c]pyrrole-4,6-dione[35] π-acceptor units. Therefore, from synthetic chemistry and materials design perspectives, the development of new π-acceptor building blocks is of great importance to diversify the chemistry of charge-transporting polymeric materials and to realize novel properties in advanced optoelectronic technologies.

BODIPY (4,4-difluoro-4-bora-3a,4a-diaza-*s*-indacene) π-core, structurally considered as "porphyrin's little sister," has attracted significant interest because of its potential technological applications in various fields including biochemical labeling,

M. Ozdemir, Prof. H. Usta
Department of Materials Science and Nanotechnology Engineering
Abdullah Gül University
Kayseri 38080, Turkey
E-mail: hakan.usta@agu.edu.tr
S. W. Kim, Prof. B. J. Kim
Department of Chemical and Biomolecular Engineering
Korea Advanced Institute of Science and Technology (KAIST)
Daejeon 34141, Republic of Korea
E-mail: bjkim02@kaist.ac.kr
H. Kim, Prof. C. Kim
Department of Chemical and Biomolecular Engineering
Sogang University
Mapo-gu, Seoul 04107, Republic of Korea
E-mail: choongik@sogang.ac.kr
Prof. M.-G. Kim
Department of Chemistry
Chung-Ang University
Dongjak-gu, Seoul 06974, Republic of Korea
The ORCID identification number(s) for the author(s) of this article can be found under https://doi.org/10.1002/aelm.201700354.

DOI: 10.1002/aelm.201700354

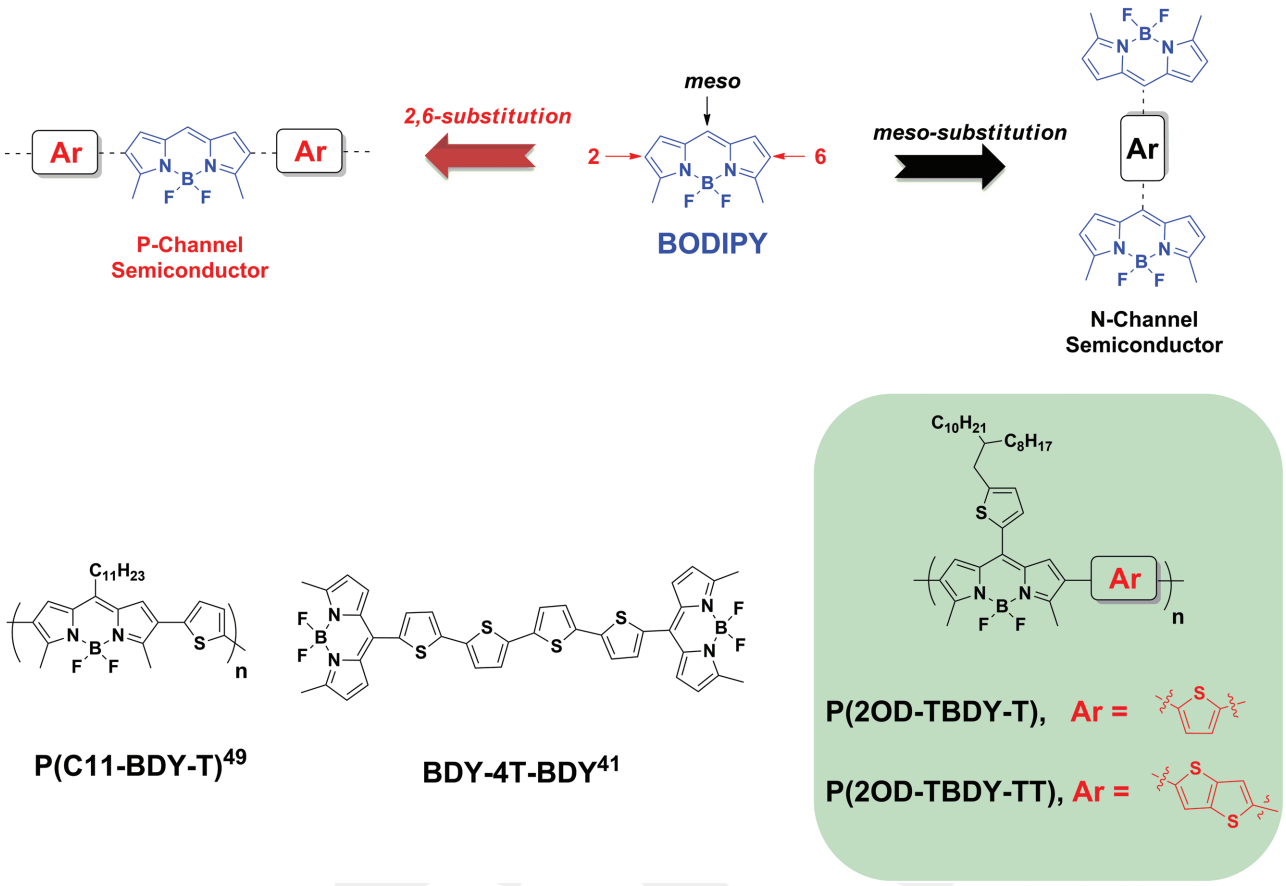

Figure 1. The effect of aromatic substitutions at *meso*- and 2,6-positions of the BODIPY π-core on the charge-carrier type, the chemical structures of previously developed semiconductors **P(C11-BDY-T)**[49] and **BDY-4T-BDY**,[41] and the copolymers **P(2OD-TBDY-T)** and **P(2OD-TBDY-TT)** developed in this study.

fluorescent switching, and photodynamic therapy.[41–45] Recently, BODIPY-based semiconductors are attracting considerable attention for their applications in the organic electronics.[46–48] This is not only due to BODIPY π-core's facile synthesis/modification but also because of its advantageous structural/electronic properties such as coplanarity, energetically stabilized lowest unoccupied molecular orbital (LUMO) level, good solubility, and high dipole moment.[41,49–55] To this end, it has been recently demonstrated by several research groups that BODIPY has a very unique electronic structure and that its charge-carrier type is highly dependent on its π-architecture.[56–58] While π-extension on BODIPY's *meso*-position leads to n-channel semiconductivity (as in the case of **BDY-4T-BDY**, μ_e = 0.01 $cm^2\ V^{-1}\cdot s^{-1}$),[41,58] aromatic substitutions on 2,6-positions yield p-channel semiconductors (**Figure 1**).[49] By means of this unique electronic feature, some of us have recently demonstrated solution-processed p-channel OFETs based on a semicrystalline BODIPY–thiophene copolymer **P(C11-BDY-T)** (Figure 1),[49] which is still holding the record for charge-carrier mobility (μ_h = 0.17 $cm^2\ V^{-1}\cdot s^{-1}$) among all known BODIPY-based semiconductors. In these studies, BODIPY core stands out as a promising, highly electron-deficient, and versatile π-acceptor building block with superior solution processability. However, BODIPY-based donor polymers still show very poor solar cell performances with PCEs of only ≈1–2% in fullerene-based BHJ devices.[47,59–61] The reported solar cells consisting of BODIPY-based polymers and [6,6]-phenyl C61/71 butyric acid methyl ester (PCBM) suffered from one or more of these following complications: low short-circuit current (J_{SC}) mainly due to poor solubility of polymer donors, mismatched energy levels, and unoptimized BHJ morphology with fullerene acceptors, which prevents efficient charge transport and generation. Therefore, further research is required to design and develop new polymerizable BODIPY-based building blocks and to investigate their properties in semiconducting copolymers for use in OPVs and OFETs. To this end, the development of BODIPY-based polymers, which can yield high PCEs in inverted solar cell device structure, is especially very important. This is because, compared with conventional BHJ-OPV devices, inverted structure has the advantage of improved long-term ambient stability since corrosive/hygroscopic hole-transporting poly(3,4-ethylen edioxylenethiophene):poly(styrenesulfonicacid) (PEDOT:PSS) and low-work-function metal cathode are not needed, and these devices are self-encapsulated.[22,23,62]

In this paper, a highly electron-deficient and soluble *meso*-heteroaromatic substituted π-acceptor building block, **2OD-TBDY-Br$_2$** (**Scheme 1**), is developed. When compared with *meso*-alkyl substituted BODIPY monomers, π-delocalization

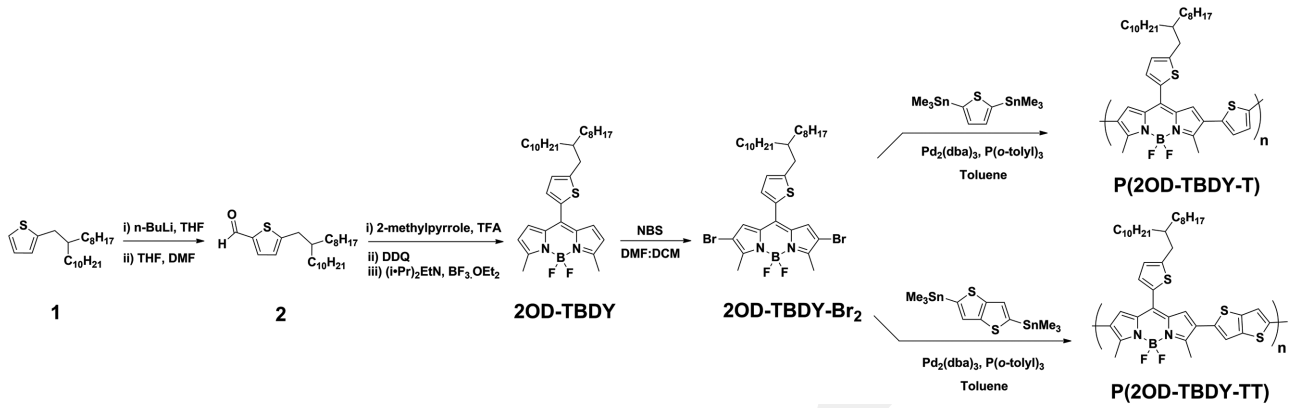

Scheme 1. Synthesis of *meso*-thiophene substituted monomer **2OD-TBDY-Br$_2$** and the corresponding copolymers **P(2OD-TBDY-T)** and **P(2OD-TBDY-TT)**.

for the LUMO in this building block is found to be extended toward the *meso*-thienyl π-core, which yields highly favorable structural/electronic properties. Based on the previous findings that *meso*-heteroaromatic substituted BODIPY π-systems are efficient electron-transporting semiconductors, we envision a similar rationale that *meso*-heteroaromatic substitutions on BODIPY-based monomers may lead to enhanced electron-acceptor characteristics.[41,58,63] **2OD-TBDY-Br$_2$** was copolymerized with thiophene and thieno[3,2-b]thiophene donor moieties to yield two new low band-gap (E_g = 1.31–1.35 eV) donor–acceptor semiconducting copolymers **P(2OD-TBDY-T)** and **P(2OD-TBDY-TT)**, respectively (Figure 1). The polymeric semiconductor thin films prepared by spin coating show isotropic nodule-like grains with essentially no microstructural ordering in the out-of-plane direction. The polymer solutions and the corresponding thin films exhibit strong aggregation-dependent excitonic properties, as studied by temperature-dependent UV–vis absorption spectroscopy. Enhanced π-coherence was evident in solution even at high temperature as a result of strong interchain interactions. OFETs in bottom-gate/top-contact device geometry featuring polymer semiconductor thin films demonstrate hole mobilities of 0.005 $cm^2\ V^{-1}\cdot s^{-1}$ and 0.0002 $cm^2\ V^{-1}\cdot s^{-1}$ for **P(2OD-TBDY-T)** and **P(2OD-TBDY-TT)**, respectively, with I_{on}/I_{off} ratios of 10^4–10^6 in ambient. BHJ-OPVs consisting of **P(2OD-TBDY-T)** donor polymer and $PC_{71}BM$ acceptor had the PCE of 6.16% with high J_{SC} value of 16.63 mA cm^{-2}. To the best of our knowledge, the PCE value is the highest achieved to date for the OPVs based on BODIPY-based donor polymer, and, more generally, on the boron-containing donor polymers.

2. Results and Discussion

2.1. Computational Design, Synthesis, and Characterization

Explored via computational modeling, the structural and electronic properties of the building block, **2OD-TBDY**, were found to be highly attractive for a strong π-acceptor building block. Note that the molecular structure of **2OD-TBDY** monomer developed herein employs an alkyl substituent modification of an original *meso*-thiophene substituted BODIPY monomer reported by Chochos et al.[47] In the structure of **2OD-TBDY**, five-membered thienyl aromatic unit is placed at *meso*-position to minimize the dihedral angle ($\theta_{Th\text{-}BODIPY}$ ≈47°) with highly coplanar dipyrromethene π-core. This is consistent with the previously measured thienyl-dipyrromethene dihedral angles ($\theta_{Th\text{-}BODIPY}$ ≈ 45°–48°) in single-crystal structures, and it could contribute to efficient π–π stacking and C—H$\cdots\pi$ interactions in the copolymer solid state.[41,63] As shown in **Figure 2**, π-delocalization of the LUMO frontier orbital is found to be extended toward the *meso*-thienyl unit, which results in lowered LUMO energy (–2.48 eV → –2.64 eV) as compared to the alkyl-substituted monomer **C11-BDY**. As expected, the highest occupied molecular orbital (HOMO) energy level remains the same (≈–5.50 eV) since the corresponding π-electron density is found to be delocalized only on the boron-dipyrromethene π-core. Thus, the HOMO–LUMO gap for **2OD-TBDY** is found to be reduced by ≈0.16 eV as compared to that of **C11-BDY**. On the other hand, the presence of thienyl unit at *meso*-position significantly increases the magnitude of the ground-state dipole moment from 3.83 D (for **C11-BDY**) to 4.75 D (**2OD-TBDY**) while the direction remains the same pointing toward the 4,4′-difluorine substituents. This could enhance backbone-ordering and interchain interactions in the corresponding copolymer thin films as a result of strong dipolar interactions.[64] In order to demonstrate that improved acceptor property of **2OD-TBDY** could translate into donor–acceptor type π-backbones, we performed density functional theory (DFT) calculations on D–A–D model units (**T-C11-BDY-T** and **T-2OD-TBDY-T** in Figure S1 in the Supporting Information) by employing thiophene donors at 2,6-positions of the BODIPY unit. These results also demonstrate energetically stabilized and delocalized LUMO, and reduced band gap for **2OD-TBDY-**based D–A–D system as compared with that based on *meso*-alkyl substituted **C11-BDY** acceptor. Furthermore, according to recent findings by L. Yu et al.[65] and J. Hou et al.[29] on fluorinated small molecules and polymers, fluorination increases ground-state dipole moment and yields higher π-system polarization, which effectively lowers the exciton Coulomb binding energy and leads to faster charge separation kinetics in photovoltaics. Therefore, we envision that the new D–A copolymers employing **2OD-TBDY** π-acceptor may show improved photovoltaic performances in BHJ devices. Sterically encumbered swallow-tailed alkyl substituent

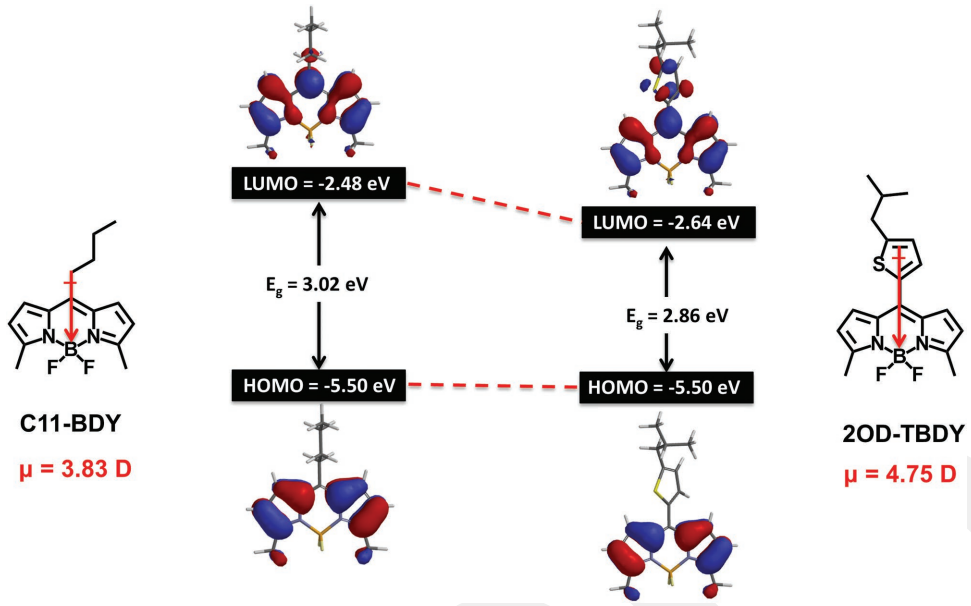

Figure 2. Calculated frontier molecular orbital (HOMO/LUMO) energy levels and pictorial representations, and molecular dipole moments (μ) of model monomers for *meso*-alkyl substituted **C11-BDY**[49] and *meso*-thiophene substituted **2OD-TBDY** developed in this study (B3LYP/6-31G** level of theory).

(2-octyldodecyl) is placed at α-position of the *meso*-thienyl unit, which provides increased solubility to the corresponding copolymers while keeping the insulating C—C/C—H σ-bonds further away from the semiconducting π-system. This type of structural strategy of physically separating σ-alkyl chain and π-system has recently been shown to yield efficient charge-transport properties in isoindigo-based copolymers.[66] From a structural and electronic standpoint, **2OD-TBDY** has much improved π-acceptor characteristics as compared to *meso*-alkyl substituted BODIPY monomer **C11-BDY** (Figure 2), and it has similar properties to some of the commonly known electron-deficient building blocks (dithienyldiketopyrrolopyrrole (T-DPP-T) (LUMO = −2.50 eV, μ = 0.15 D); isoindigo (LUMO = −2.64 eV, μ = 0.49 D); naphthalenediimide (LUMO = −3.37 eV, μ = 0 D); Figure S2, Supporting Information), which were reported to yield low band-gap polymers.[67–69] Therefore, we envision that **2OD-TBDY** building block should be a promising π-acceptor for use in low band-gap semiconducting copolymer backbones.

The synthetic routes to the **2OD-TBDY-Br$_2$** monomer, and its corresponding copolymers **P(2OD-TBDY-T)** and **P(2OD-TBDY-TT)**, are shown in Scheme 1. 5-(2-octyldodecyl)-2-thiophenecarboxaldehyde compound **2** was prepared in two steps (40% total yield) by first lithiation/alkylation of thiophene at 5-position to give compound **1**, which was subsequently lithiated and reacted with dimethylformamide (DMF) to form the carboxaldehyde functionality at 2-position. The boron-dipyrromethene π-core **2OD-TBDY** was prepared by reacting 5-(2-octyldodecyl)-2-thiophenecarboxaldehyde (**2**) with 2-methyl pyrrole in the presence of a catalytic amount of trifluoroacetic acid (TFA), which was subsequently oxidized with 2,3-dichloro-5,6-dicyano-1,4-benzoquinone (DDQ) and coordinated with trifluoroborane diethetherate ($BF_3 \cdot OEt_2$) in the presence of (i-Pr)$_2$EtN (28% yield). Bromination at the 2- and 6-positions was selectively accomplished with *N*-bromosuccinimide, which afforded the dibromo-functionalized BODIPY monomer **2OD-TBDY-Br$_2$** in 91% yield. The chemical structures and purities of the intermediate compounds and the resulting monomer, **2OD-TBDY-Br$_2$**, were characterized by ^{1}H/^{13}C NMR (Figures S3, S4, S6, and S7, Supporting Information), matrix assisted laser desorption ionization-time of flight mass spectrometry (MALDI-TOF) (Figures S5 and S8, Supporting Information), and elemental analysis. Stille polycondensation protocols were employed for the copolymerization reactions of **2OD-TBDY-Br$_2$** with 2,5-bis(trimethylstannyl)thiophene and 2,5-bis(trimethylstannyl)thieno[3,2-b]thiophene in toluene using $Pd_2(dba)_3$/P(o-tolyl)$_3$ as the catalyst/ligand system. During the copolymerization of **2OD-TBDY-Br$_2$** with 2,5-bis(trimethylstannyl) thieno[3,2-b]thiophene, the reaction was stopped after 5 min; otherwise, the copolymers were found to be insoluble. The obtained **P(2OD-TBDY-T)** and **P(2OD-TBDY-TT)** solids were purified by sequential Soxhlet extractions (methanol–acetone–hexane) and multiple dissolution–precipitation processes with methanol/chloroform to yield dark-colored solids in 91% and 20% yields, respectively. The copolymers' purities were evaluated by elemental analysis and molecular weights were determined by gel permeation chromatography (GPC) with tetrahydrofuran (THF) as the eluent against polystyrene standards, which indicated number-average molecular weights (M_n) of 75.3 kDa for **P(2OD-TBDY-T)** and 11.0 kDa for **P(2OD-TBDY-TT)**. The relatively lower molecular weight of **P(2OD-TBDY-TT)** can be explained by the fact that the corresponding polymerization reaction was stopped at its earlier stage to obtain a soluble polymer. The good solubility of the current copolymers should enable the solution-based fabrication of copolymer thin films for use in BHJ-OPV and OFET devices. Both copolymers show good thermal stabilities with decomposition onset temperatures (5% mass loss) at 372°–384 °C (Figure S9, Supporting Information). No apparent phase transitions were observed for both copolymers in the range of 25° to 350 °C by differential scanning calorimetry (DSC).

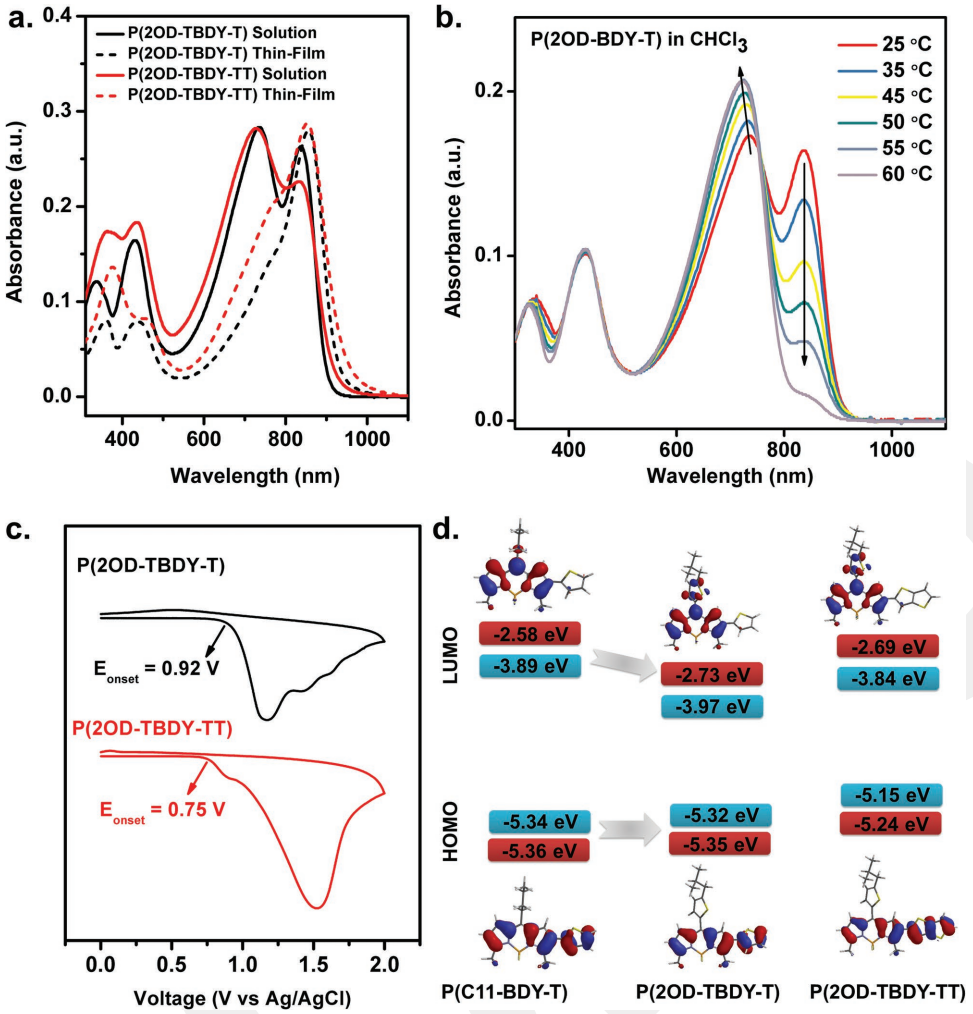

Figure 3. a) Optical absorption spectra in chloroform (solid lines, 1.0×10^{-5} M) and as spin-coated thin films on glass (dashed lines) for copolymers **P(2OD-TBDY-T)** and **P(2OD-TBDY-TT)**. b) Temperature-dependent UV–vis absorption spectra of **P(2OD-TBDY-T)** in chloroform solution (0.6×10^{-5} M) (arrows indicate the trends upon temperature increases). c) Cyclic voltammograms as thin films in 0.1 M $TBAPF_6$/MeCN solution versus Ag/AgCl (3.0 M NaCl) at a scan rate of 100 mV s^{-1}. d) Energy diagrams showing theoretically calculated (red) (for model monomers) and experimentally estimated (blue) HOMO/LUMO energy levels as well as their topographical representations. Note that P(C11-BDY-T) is our previously reported BODIPY-based copolymer.[49]

2.2. Optoelectronic Characterizations

The optical characteristics of the new copolymers were studied by UV–vis absorption spectroscopy in dilute solutions ($CHCl_3$, 10^{-5} M) and thin-film states (as spin-coated thin films on glass). As shown in **Figure 3**a, the copolymers exhibit two low-energy absorption maxima at 838/736 nm for **P(2OD-TBDY-T)** and 834/730 nm for **P(2OD-TBDY-TT)** corresponding to π–π^* excitations. In order to elucidate the origin of these peaks, which are separated by ≈0.2–0.3 eV, temperature-dependent UV–vis absorption spectra of the current polymers were recorded in chloroform and toluene solutions. As shown in Figure 3b, upon progressive heating (25° → 60 °C) of **P(2OD-TBDY-T)** solution in chloroform, while the absorbance at the lower energy peak (838 nm) greatly decreases, the absorbance at the higher energy peak (736 nm) gradually increases with a blue-shift of ≈12 nm. In addition, an isosbestic point was observed at 756 nm. Likewise, the chloroform solution of **P(2OD-TBDY-TT)** exhibits similar trends but with much smaller changes in absorbance values (Figure S10a, Supporting Information), which indicates the difference between the polymers' temperature-dependent aggregation behaviors. Based on these results, we assign the absorbance at higher energy peak (736 and 730 nm) to disaggregated (isolated) polymer chains and the absorbance at lower energy peak (838 and 834 nm) to aggregated polymer chains in solution (enhanced π-coherence as a result of interchain interactions). On the other hand, when high-boiling point solvent (i.e., toluene) was used for **P(2OD-TBDY-T)**, the presence of higher-energy shoulder even at 85 °C indicates strong aggregation tendency of the current D–A copolymer in toluene even at high temperature (Figure S10b, Supporting Information). Note that **P(2OD-TBDY-TT)** solution in toluene shows mostly disaggregated (isolated) polymer chains and the aggregation peak almost disappears at 85 °C (Figure S10c, Supporting Information).

When BODIPY acceptor, **2OD-TBDY**, is copolymerized with thiophene-based donors (i.e., T and TT) through 2,6-positions, the corresponding absorption profiles were found to significantly red-shift ($\Delta\lambda_{max} \approx 315$ nm and $\Delta\lambda_{onset} \approx 360$ nm in Figure S11 in the Supporting Information), which indicates highly extended electronic communication (effective π-conjugation) between BODIPY-based acceptor and thiophene-based donor units along the current polymer backbones. This is in sharp contrast to the observations on BODIPY-oligothiophene π-systems, since they exhibit very limited electronic communications between boron-dipyrromethene and oligothiophene moieties when linked through BODIPY's *meso*-position.[41,63] Note that, when the new copolymer **P(2OD-TBDY-T)** is compared with structurally related **P(C11-BDY-T)** (Figure 1),[49] the low-energy absorption maxima and onset were found to be significantly red-shifted ($\Delta\lambda_{max} \approx 136$ nm; $\Delta\lambda_{onset} \approx 75$ nm), indicating more favorable electronic/structural properties of the new acceptor unit (**2OD-TBDY**) to enhance π-conjugation, donor–acceptor interactions, and aggregation (interchain interactions).

The absorption maximum for spin-coated copolymer thin films are significantly red-shifted ($\Delta\lambda_{max} \approx 120$ nm) compared to those in chloroform solution. For both copolymers, going from solution to solid state, the lower-energy aggregation peak becomes stronger and the disaggregation absorbance becomes a shoulder peak, which suggests the existence of strong interchain interactions (enhanced π-coherence) in the solid state. The solid-state optical band gaps are estimated from the low-energy band edges as 1.35 and 1.31 eV for **P(2OD-TBDY-T)** and **P(2OD-TBDY-TT)**, respectively. These low optical bands make the new copolymers quite attractive for various optoelectronic applications.[11] The observed aggregation properties both in solution and solid state for the present copolymers could be attributed to strong interchain interactions (π–π stacking, donor–acceptor, and dipolar) between polymer chains, resulting in enhanced π-coherence. Similar temperature-dependent aggregation behaviors in solution and strong aggregations in solid state were previously reported for several donor–acceptor copolymers characterized in high-performing BHJ-OPVs based on isoindigo,[70] B ← N bridged bipyridine,[71] naphthalene diimide,[68] and difluorobenzothiadiazole[24] acceptors.

We also studied the aggregate formation via solvent-dependent absorption spectra by adding a nonsolvent (ethanol, $\varepsilon = 24.5$) to a well-dissolved copolymer solution in chloroform. As shown in **Figure 4**, both copolymers show gradual reduction of the intensities for the higher-energy peaks at 730/736 nm

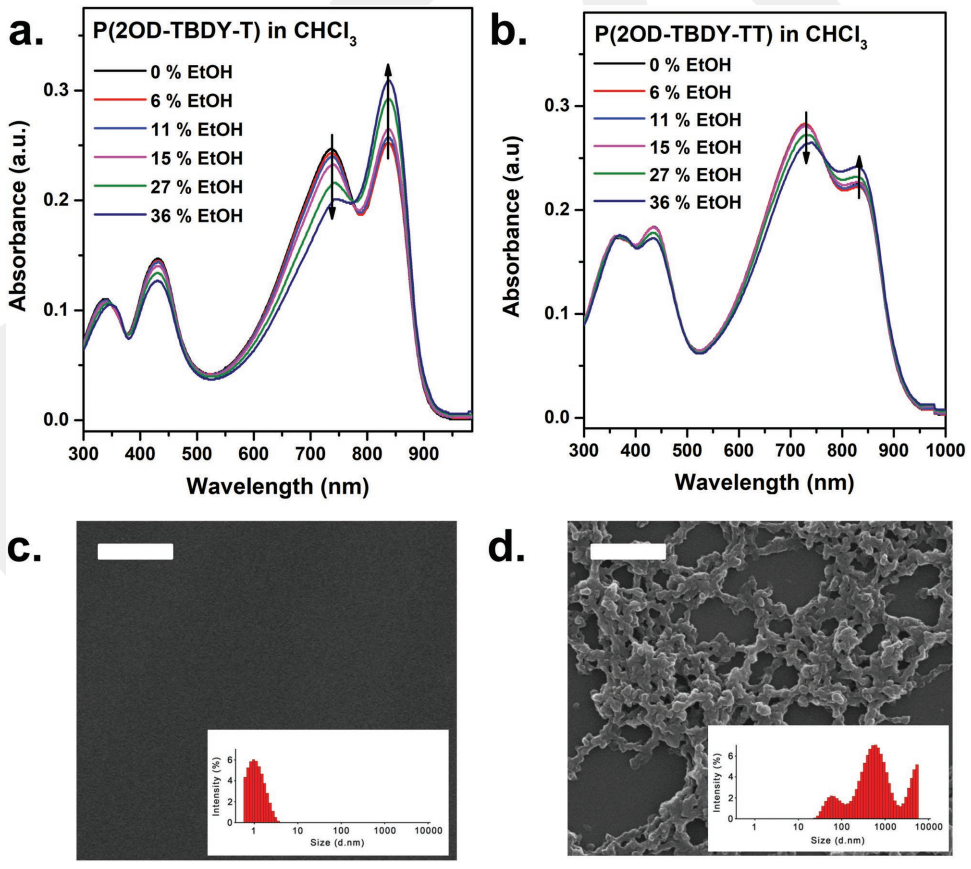

Figure 4. Solvent-dependent optical absorption spectra of a) **P(2OD-TBDY-T)** and b) **P(2OD-TBDY-TT)** in chloroform–ethanol mixtures at room temperature starting in pure chloroform (black line) and successively increasing the volume fraction (from 0% to 36%) of ethanol. Arrows indicate the spectral changes upon nonsolvent addition. SEM images for P(2OD-TBDY-T) films drop-casted on Si(100) from c) chloroform and d) chloroform:ethanol (64:36, v/v) solutions. Insets show the size distributions of the corresponding drop-casting solutions determined by DLS. Scale bars denote 1 µm.

and concurrent increase in the intensities of the lower-energy peaks at 834/838 nm. These spectral changes were successively controlled by continually increasing the volume fraction of ethanol from 0% to 36%, and well-defined isosbestic points were observed for both copolymers at 764/774 nm, indicating that aggregation occurs under thermodynamic control.[72,73] Similar aggregation behavior was also observed when a different nonsolvent (hexane) and a bad solvent (THF) having relatively lower dielectric constants (ε_{hexane} = 2.0; ε_{THF} = 7.6) were added to copolymer solutions in chloroform (Figure S12, Supporting Information), indicating that the dielectric constant of the added solvent does not play a major role in aggregation mechanism. Next, we analyzed the suspended aggregated particle size of **P(2OD-TBDY-T)**, formed in aggregated solution, by dynamic light-scattering (DLS) technique, which indicates a significant increase in average particle size upon ethanol addition (insets in Figure 4c,d). In order to obtain more information on these aggregates, the corresponding solutions were drop-casted on Si(100) and their morphologies were determined by scanning electron microscopy (SEM). As shown in Figure 4c,d, while the film drop-casted from chloroform solution shows a very smooth morphology with no observable microscopic aggregates, the film drop-casted from chloroform:ethanol (64:36, v/v) shows a 3D polymeric network consisting of nanoparticles and micron-sized aggregates with sizes ranging from ≈50–100 nm to >1 μm, which is consistent with the DLS particle size distribution (Figure 4d inset). Thus, we propose that these particulates observed in the SEM image are mostly formed in the chloroform–ethanol solution; they are not purely based on polymer precipitation during solvent evaporation in drop casting. Note that this type of 3D micro/nanostructured organic surface morphologies, which can be prepared via simple solution processing, might be quite advantageous for low-cost surface-enhanced Raman scattering platforms and catalysis applications.[74]

The cyclic voltammograms of the **P(2OD-TBDY-T)** and **P(2OD-TBDY-TT)** copolymeric films drop-casted on platinum electrodes are shown in Figure 3c. The measurements are performed in 0.1 M $TBAPF_6$ solution in acetonitrile against Ag/AgCl (3.0 M NaCl) reference electrode. For **P(2OD-TBDY-T)** and **P(2OD-TBDY-TT)**, only oxidation peaks are observed and the onset of the oxidation potentials are located at 0.92 V (vs Ag/AgCl) and 0.75 V (vs Ag/AgCl), respectively, from which solid-state HOMO energies are estimated as −5.32 and −5.15 eV, respectively. The solid-state LUMO energies are estimated using the thin-film optical bandgaps as −3.97 eV for **P(2OD-TBDY-T)** and −3.84 eV for **P(2OD-TBDY-TT)**. When the energy levels of **P(2OD-TBDY-TT)** are compared with those of **P(2OD-TBDY-T)**, the increases ($\Delta \approx$ 0.15 eV) in both HOMO and LUMO energies reflect relatively more π-extended electronic structure of thieno[3,2-b]thiophene donor unit versus thiophene. On the other hand, for the copolymers embedding the same thiophene donor unit, the new copolymer **P(2OD-TBDY-T)** has a relatively lower LUMO energy level and similar HOMO energy level as compared to the previously reported copolymer **P(C11-BDY-T)**,[49] which reflects better electron-acceptor characteristics of the new building block **2OD-TBDY** as compared to **C11-BDY**. All these trends in the experimental HOMO/LUMO energy levels (blue) correlate well with the theoretically calculated values (red) on the model repeating units (Figure 3d). It is noteworthy that the HOMO energies of the current copolymers are typical of ambient-stable p-channel semiconductors.[11] However, although LUMO energies of these copolymers are quite stabilized and they are even in the energetic regime of the ambient-stable n-channel semiconductors (≤−3.8 eV), no electron transport was observed under vacuum and in ambient (vide infra).

2.3. Thin-Film Fabrication, Characterization, and Field-Effect Transistor Devices

The semiconductor characteristics of the current copolymers **P(2OD-TBDY-T)** and **P(2OD-TBDY-TT)** were studied in OFETs in a bottom-gate/top-contact (BG-TC) device architecture. The semiconductor thin films (≈50–60 nm) were prepared by spin coating copolymer solutions (5–7 mg mL^{-1} in chloroform) on PS-brush treated n^{++}-Si/SiO_2(300 nm) gate-dielectric substrates, which was followed by drying at 70 °C under vacuum to remove residual solvents. Note that this temperature is an acceptable temperature for industrial applications and no further thermal annealing is needed. The reason for dielectric surface functionalization with PS brushes was to achieve a favorable semiconductor–dielectric interface.[75] Polymeric thin-film microstructures and morphologies were studied by θ–2θ X-ray diffraction (XRD) and atomic force microscopy (AFM). As shown in **Figure 5**a,b, XRD profiles do not exhibit any low-angle ($2\theta < 10°$) diffraction peak, which indicates the lack of lamellar crystalline regions in the out-of-plane direction.[76] For both polymer thin films, the only noticeable diffractions show highly broadened peaks centered at $2\theta \approx 22°$. Since the reference XRD scan on pristine PS-brush treated n^{++}-Si/SiO_2 (300 nm) substrate does not exhibit similar broadened peak, these peaks are assigned to short-range ordered π–π interactions originating from the polymer semiconductor film. This corresponds to π–π stacking distances of ≈4.0 Å.[22,77] Indeed, the XRD profiles obtained for the current copolymers could be attributed to the presence of bulkyl swallow-tailed 2OD alkyl substituents on BODIPY unit, which prevents the formation of lamellar ordering in the out-of-plane crystallographic direction.[76,78,79] These microstructural observations agree well with the AFM characterizations, which reveal relatively homogeneous morphologies with extremely smooth surfaces (root-mean-square roughness <1 nm for 5.0 μm × 5.0 μm scan area). As shown in Figure 5c,d, both films show highly interconnected isotropic nodule-like domains (≈50–100 nm in diameter). OFET device characteristics are measured in ambient conditions, and typical transfer and output plots are shown in Figure 5e and Figure S13 in the Supporting Information. Consistent with the prefabrication theoretical and experimental optoelectronic characterizations, these devices exhibit unipolar p-channel operation with μ_h = 0.005 $cm^2\ V^{-1}\cdot s^{-1}$ ($I_{on}/I_{off} = 10^4$–10^5) and $\mu_h = 0.0002\ cm^2\ V^{-1}\cdot s^{-1}$ ($I_{on}/I_{off} = 10^4$–10^6) for **P(2OD-TBDY-T)** and **P(2OD-TBDY-TT)**, respectively. Note that these devices were dried/annealed only at 70 °C, and post-deposition thermal annealing at higher temperatures did not further improve the transistor performance

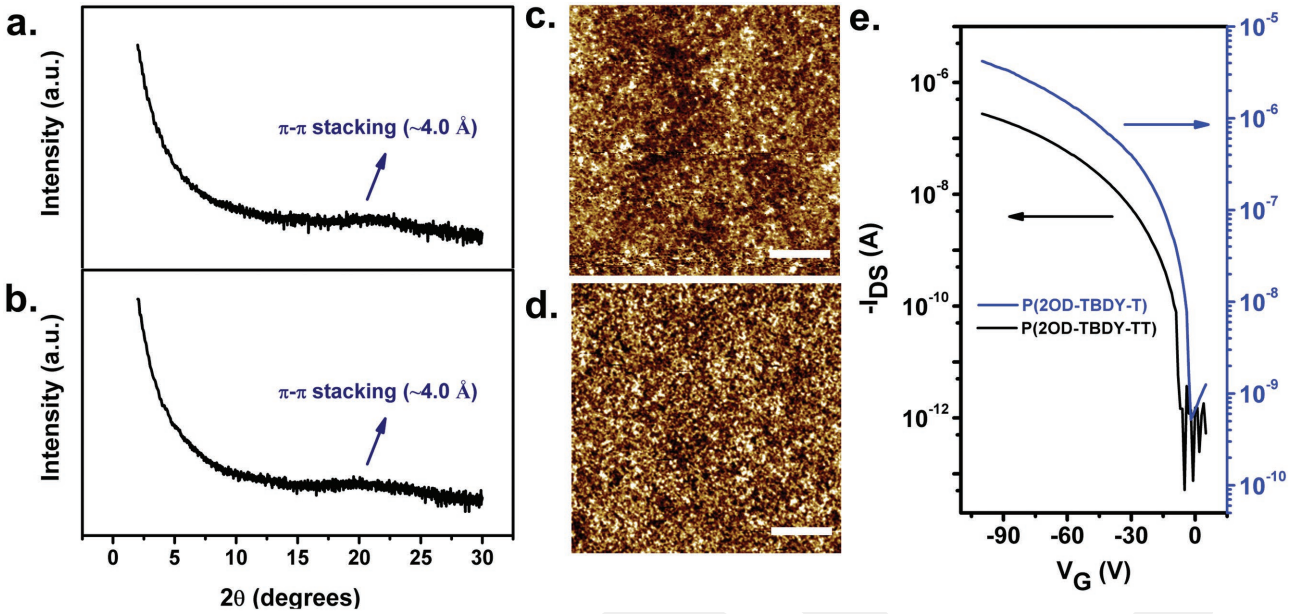

Figure 5. θ–2θ XRD scans and AFM topographic images for spin-coated thin films of a,b) **P(2OD-TBDY-T)** and b,d) **P(2OD-TBDY-TT)**. e) P-channel transfer curves (V_{DS} = −100 V) for bottom-gate/top-contact OFET devices fabricated with spin-coated copolymer thin-films. Scale bars in AFM images denote 1 µm.

as well as the polymer crystallinity/morphology. Since no evident microstructural and morphological differences were revealed between two polymer thin films, the inferior device performance of **P(2OD-TBDY-TT)**, as compared with **P(2OD-TBDY-T)**, should originate from its much lower molecular weight (M_n = 11.0 vs 75.3 kDa).[80] From frontier-orbital energetics perspective, one would expect the current copolymers to exhibit also n-channel semiconductivity, because the present LUMOs are in the energetic range of those measured for typical n-channel semiconductors.[11,81,82] Therefore, we performed DFT calculations on trimer and tetramer models of the repeating units, which shows localization on specific BODIPY units for LUMO π-electron density and complete delocalization along the π-backbone for HOMO (Figure S14, Supporting Information). Therefore, it seems that the major charge-carrier type (hole vs electron) of the current polymers is directed by the corresponding π-orbital distributions. Note that the semiconductivity in polymeric films will occur mainly through intra- and interchain charge transports, which relies on the formation of radical cationic species (polarons) on isolated and aggregated conjugated segments of the polymer chains, respectively.[83] Therefore, it is quite crucial to have highly π-conjugated polymer chains with good interchain interactions in the solid state, which agrees well with the current polymeric thin films. Since the length of a single copolymer chain—even in its fully extended conformation—is much smaller than the device channel lengths (≈50–100 µm), π–π stacked regions are still very crucial to enable interchain hopping processes for an efficient charge transport from source to drain. Although the current charge-carrier mobilities are short of the state-of-the-art performances recently achieved with D–A copolymers, they are among the highest for BODIPY-based semiconductor polymers measured in BG-TC OFETs.

2.4. Bulk-Heterojunction Inverted Solar Cell Devices

Next, we investigated the photovoltaic performance of **P(2OD-TBDY-T)** as polymer donor by fabricating the inverted bulk-heterojunction (BHJ) solar cells with a device architecture of ITO/ZnO/active layer (**P(2OD-TBDY-T)**:$PC_{71}BM$)/MoO_3/Ag (see the Experimental Section for device fabrication details). The inverted device structure was preferred due to better device stability in air when compared with the normal-type structure. This is because high work-function metal anodes (resistant to oxidation in air) are used in inverted structures and acidic PEDOT:PSS layer is not required, which leads to much superior long-term stability.[84–86] The optimal polymer:fullerene blend weight ratio in the active layer was found to be 1:1.5 (w/w), and chloroform was used as the processing solvent. In general, the addition of solvent additives optimizes the BHJ morphology, which plays a crucial role in determining the corresponding device performance.[87] Therefore, we studied **P(2OD-TBDY-T)**:$PC_{71}BM$ device characteristics with or without 1,8-diiodooctane (DIO) additive in the processing solvent. **Figure 6** shows the *J*–*V* curves and external quantum efficiency (EQE) responses of the devices under AM 1.5G illumination (100 mW cm^{-2}), and the corresponding photovoltaic parameters are summarized in **Table 1**. The devices without DIO additive exhibited an impressive PCE of 5.12% with V_{oc} of 0.73 V, J_{sc} of 13.08 mA cm^{-2}, and fill factor (FF) = 0.53. The devices with 3 vol% DIO additive showed further improved photovoltaic performance with PCE of 6.16%, V_{oc} of 0.66 V, J_{sc} of 16.36 mA cm^{-2}, and FF = 0.56, which is a record high PCE value among the solar cells based on BODIPY-polymer donor. Although the use of the DIO additive resulted in a slight decrease of V_{oc} value by ≈10%, the J_{sc} value was increased by ≈27%, resulting in a significant improvement (≈20%) in the PCE value. The

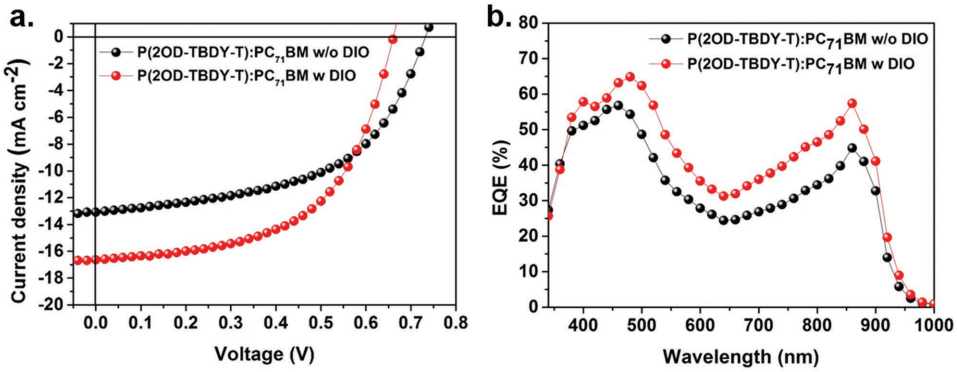

Figure 6. a) *J–V* characteristics and b) EQE responses of **P(2OD-TBDY-T)**:$PC_{71}BM$ without or with DIO additive.

decrease of V_{oc} and the increase of J_{sc} are fairly common for the active layer film processed with DIO additive in polymer solar cells reported to date.[88–93] To support these changes in V_{oc} and J_{sc} values after the addition of DIO additive, we measured the absorption spectra of the P(2OD-TBDY-T):$PC_{71}BM$ blend films without or with DIO additive (Figure S15, Supporting Information). It was clearly observed that absorption peak of the blend film with DIO additive increased in intensity in the range of 800–900 nm, and slightly red-shifted from 849 to 855 nm, indicating an increased structural ordering and interchain interactions for polymer donor.[94–96] The variations of the absorption spectra for blend films without and with DIO additive were closely correlated with the photovoltaic parameters of the devices. As shown in Figure 6b, the **P(2OD-TBDY-T)**:$PC_{71}BM$ devices were observed to effectively generate photocurrent in a broad spectral range of 400–900 nm. The active layer with DIO additive showed higher EQE values than that without DIO additive in the entire spectral range, even leading to maximum EQE values of >65% at 450–500 nm. The J_{sc} values calculated from EQE spectrum of **P(2OD-TBDY-T)**:$PC_{71}BM$ without and with DIO additive were 12.53 or 15.87 mA cm^{-2}, respectively, which agree well with the corresponding J_{sc} values from *J–V* curves within an acceptable error of ≈5%. The hole (μ_h) and electron (μ_e) mobilities of the **P(2OD-TBDY-T)**:$PC_{71}BM$ with DIO additive device were measured by the space-charge limited current (SCLC) method under optimized device condition, which were calculated as 3.56×10^{-5} cm^2 $V^{-1}s^{-1}$ and 2.75×10^{-5} cm^2 V^{-1} s^{-1}, respectively. Notably, the hole and electron mobilities are well balanced ($\mu_h/\mu_e = 1.29$), which can contribute to efficient charge transport.[97]

The morphology of the polymer/fullerene blend active layer plays a critical role in device performance, and continuous interpenetrating donor–acceptor domains with limited sizes are typically needed for efficient exciton dissociation and charge-carrier transport/extraction. We compared the BHJ morphologies of **P(2OD-TBDY-T)**:$PC_{71}BM$ blend film without or with DIO additive using transmission electron microscopy (TEM) and AFM measurements (**Figures 7** and **8**). The blend film without DIO additive had continuous network of polymer donor and $PC_{71}BM$ phases, but their length scale of phase separation (i.e., large dark PCBM-rich domains (>80–110 nm)) is significantly larger than the typical exciton diffusion length of ≈10–20 nm.[98] In contrast, blend films with DIO additive exhibited highly interpenetrated domains with much decreased domain sizes (<20–40 nm), producing much larger interfacial area between **P(2OD-TBDY-T)** and $PC_{71}BM$. Importantly, the contrast between **P(2OD-TBDY-T)** and $PC_{71}BM$ is greatly enhanced, suggesting that the relative purity of each domain is higher, which is beneficial for efficient charge transport and suppressed bimolecular charge recombination in the **P(2OD-TBDY-T)**:$PC_{71}BM$ devices with DIO additive.[99,100] The observations from TEM data clearly explain the enhanced J_{sc}, FF, and PCE values of **P(2OD-TBDY-T)**:$PC_{71}BM$ devices with DIO additive.

Moreover, the AFM images (Figure 8) confirm the domain size differences between these blend films, and the blend film with DIO additive showed smaller domains with smoother surface roughness (RMS roughness = 1.1 nm) as compared to that without DIO additive (RMS roughness = 1.7 nm). To the best of our knowledge, these photovoltaic performances are the highest reported to date for a BODIPY-based donor polymer and, more generally, for a boron-containing polymer donor showing the potential of properly designed BODIPY monomer as a promising acceptor building block for OPVs. Considering that the previous research on BODIPY-based donor polymers has only achieved <1.5–2% PCEs in photovoltaic devices, the significantly enhanced photovoltaic performance (>3–4×) of the new donor polymer is mainly attributed to the well-matched energy levels with fullerene acceptors, low optical band gap, as well as the favorable BHJ morphology yielding effective charge generation and transport.

Table 1. Photovoltaic characteristics of **P(2OD-TBDY-T)**:$PC_{71}BM$ device without or with DIO additive.

Active layer [donor:acceptor]	DIO additive [3 vol%]	V_{oc} [V]	J_{sc} [mA cm^{-2}]	FF	PCE_{max} [PCE_{avg}][a)] [%]
P(2OD-TBDY-T):PC71BM	w/o	0.73	13.08	0.53	5.12(5.10)
	w	0.66	16.63	0.56	6.16(6.11)

[a)]The average PCEs were obtained from at least ten different devices for each system.

3. Conclusion

In summary, we have demonstrated the design, synthesis, and physicochemical/optoelectronic characterizations of two new

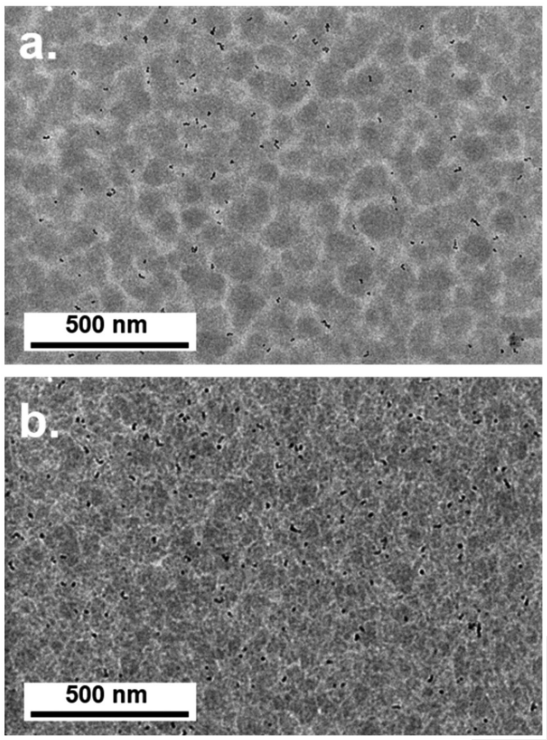

Figure 7. TEM images of **P(2OD-TBDY-T)**:$PC_{71}BM$ blend films a) without or b) with DIO additive.

low band-gap (≈1.3 eV) D–A copolymers (**P(2OD-TBDY-T)** and **P(2OD-TBDY-TT)**) based on a highly electron-deficient *meso*-thiophene substituted BODIPY π-acceptor **2OD-TBDY**. The thin films of these polymers exhibit nanoscale isotropic nodule-like domains with essentially no ordering in the out-of-plane direction. The semiconductor characteristics of the new polymers tested in BG-TC OFET devices demonstrated hole mobilities of up to ≈0.005 $cm^2\ V^{-1}\cdot s^{-1}$. By employing **P(2OD-TBDY-T)** as the electron donor and $PC_{71}BM$ as the electron acceptor in active layer, inverted BHJ-OPV devices with high PCE of ≈6.2% have been achieved. This is, to the best of our knowledge, a record high value for a boron-containing donor polymer. Since BODIPY-based polymers have only recently attracted research interest for OPV technologies, yet with much lower performances (PCEs <2%) in previous research; our findings clearly demonstrate that they can play a pronounced role in the design of high-performance donor polymers in BHJ-OPV devices.

4. Experimental Section

Materials and Methods: All reagents were used as obtained from commercial sources without any purification unless otherwise noted. Schlenk techniques were employed in the reactions by using a vacuum–nitrogen manifold system, and the reactions were carried out under N_2 unless otherwise noted. $^1H/^{13}C$ NMR spectra were recorded on a Bruker-400 spectrometer (^1H, 400 MHz; ^{13}C, 100 MHz) and thin-layer chromatography was performed on silica gel plates coated with

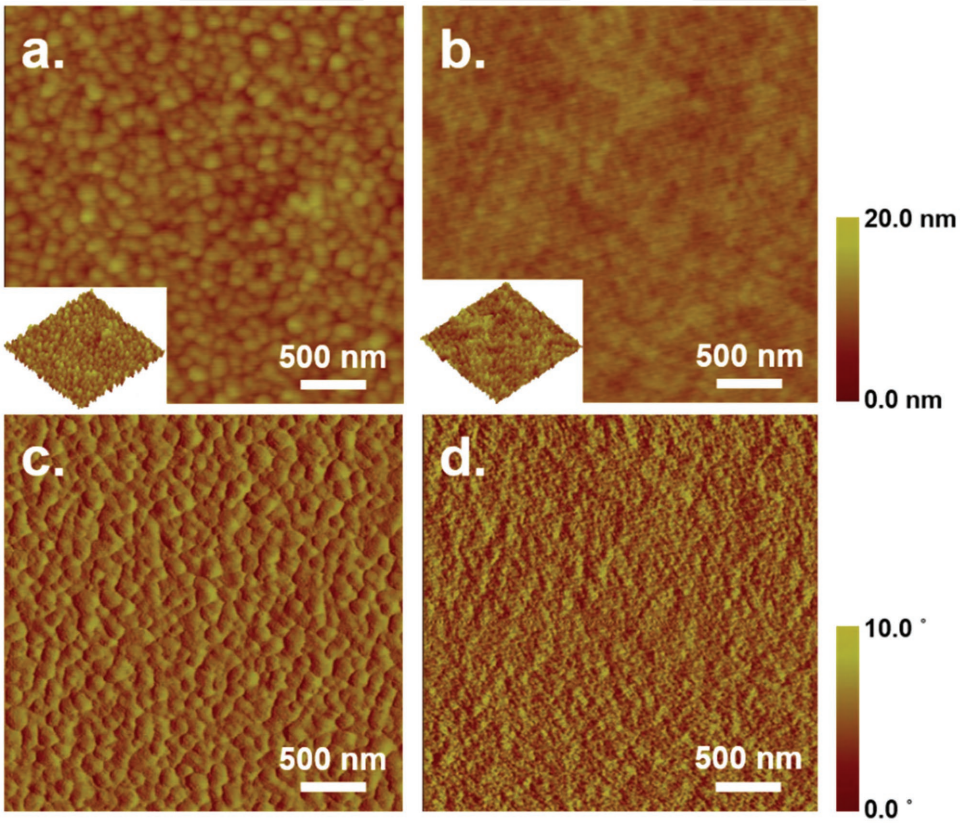

Figure 8. AFM images of **P(2OD-TBDY-T)**:$PC_{71}BM$ blend films without (a: height; c: phase) or with DIO additive (b: height; d: phase).

fluorescent indicator F254. Elemental analyses were done on a Leco Truspec Micro model instrument. MALDI-TOF characterization was performed on a Bruker Microflex LT MALDI-TOF-MS Instrument. Polymer molecular weights were determined on a Waters GPC system (Waters Pump 510) in THF at room temperature versus polystyrene standards. Thermogravimetric analysis and DSC measurements were performed on Perkin Elmer Diamond model instruments at a heating rate of 10 °C min^{-1} under nitrogen. DLS measurements were performed on a Malvern, Nano ZS Zetasizer. UV–vis absorption measurements were performed on a Shimadzu, UV-1800 UV–vis Spectrophotometer. Electrochemical measurements were performed on a C3 cell stand electrochemical station equipped with BAS-Epsilon software (Bioanalytical Systems, Inc., Lafayette, IN). The molecular geometry optimizations and total energy calculations were carried out using DFT at the B3LYP/6-31G** level by using Gaussian 09.[101]

Synthesis and Characterization: The synthesis of 2-(2-octyldodecyl) thiophene (**1**),[81] 2-methylpyrrole,[41] 2,5-bis(trimethylstannyl)-thiophene,[41] 2,5-bis(trimethylstannyl)thieno[3,2-b]thiophene,[74] and 5,5′-bis(trimethylstannyl)-2,2′-bithiophene[102] reagents were performed in accordance with the previously reported procedures.

Synthesis of 5-(2-Octyldodecyl)thiophene-2-Carbaldehyde (2): To a solution of 2-(2-octyldodecyl)thiophene (**1**) (1.7 g, 4.66 mmol) in THF (30 mL) at −78 °C 1.96 mL (4.89 mmol) of *n*-butyllithium (2.5 M in *n*-hexane) was added under nitrogen. The mixture was stirred at −78 °C for 30 min and at room temperature for 1 h. Then, *N*,*N*-dimethylformamide (0.375 g, 5.13 mmol) was added slowly at −78 °C, and the resulting reaction mixture was allowed to warm to room temperature overnight. The reaction mixture was quenched with water, and the product was extracted with hexanes. The organic phase was washed with water, dried over Na_2SO_4, filtered, and evaporated to dryness to give a crude product, which was purified by column chromatography on silica gel using hexanes:ethyl acetate (10:1) as the eluent. The pure product was obtained as a dark yellow oil (1.48 g, 81%). ^{1}H NMR ($CDCl_3$, 400 MHz): 0.89 (t, 6H, J = 6.4 Hz), 1.25–1.35 (m, 33H), 2.81 (d, 2H, J = 6.8 Hz), 6.88 (d, 1H, J = 3.6 Hz), 7.62 (d, 1H, J = 3.6 Hz), 9.83 (s, 1H).

Synthesis of 10-(5-Octyldodecylthiophen-2-yl)-5,5-Difluoro-3,7-Dimethyl-5,10a-Dihydro-1H-5l4,6l4-Dipyrrolo[1,2-c:2′,1′-f][1,3,2]Diazaborinine (2OD-TBDY): A degassed solution of 5-(2-octyldodecyl)thiophene-2-carbaldehyde (**2**) (0.70 g, 1.78 mmol) and 2-methylpyrrole (0.33 g, 4.03 mmol) in CH_2Cl_2 (≈250 mL) was prepared under nitrogen and TFA (2 drops) was added. The reaction mixture was stirred at ambient temperature overnight. Next, DDQ (0.40 g, 1.78 mmol) was added, and the reaction mixture was stirred for additional 2.5 h. Finally, *N*,*N*-diisopropylethylamine (*i*-Pr)$_2$EtN (1.26 g, 9.77 mmol) and boron trifluoride diethyl etherate ($BF_3{\cdot}Et_2O$) (0.88 g, 6.22 mmol) were added, and the reaction mixture was stirred for 2 h. The reaction mixture was poured into water and extracted with CH_2Cl_2. The organic phase was dried over Na_2SO_4, filtered, and evaporated to dryness to give a crude product, which was purified by column chromatography on silica gel using CH_2Cl_2:hexanes (2:3) as the eluent. The pure product was obtained as red oil (0.29 g, 28% yield). ^{1}H NMR (400 MHz, $CDCl_3$): δ 0.89 (t, 6H, J = 6.0 Hz), 1.27–1.33 (m, 33H), 2.66 (s, 6H), 2.82 (d, 2H, J = 6.8 Hz), 6.30 (d, 2H, J = 4.4 Hz), 6.86 (d, 1H, J = 4.0 Hz), 7.11 (d, 2H, J = 4.4 Hz), 7.29 (d, 1H, J = 4.0 Hz). ^{13}C NMR (100 MHz, $CDCl_3$): 14.1, 14.9, 22.7, 26.6, 29.3, 29.4, 29.6, 29.7, 29.8, 30.0, 31.9, 33.3, 34.7, 40.1, 119.1, 126.1, 130.3, 131.9, 132.3, 133.9, 135.4, 150.3, 157.0. MS(MALDI-TOF) *m/z* (M^+): calcd. for $C_{35}H_{53}BF_2N_2S$: 582.40, found: 582.762 $[M]^+$, 562.709 $[M\text{-}F]^+$, 534.745 $[M\text{-}F\text{-}2\times(CH_3)]^+$. Anal.calcd. for $C_{35}H_{53}BF_2N_2S$: C, 72.14; H, 9.17; N, 4.81, found: C, 72.47; H, 9.53; N, 4.98.

Synthesis of 2,8-Dibromo-10-(5-Ethylthiophen-2-yl)-5,5-Difluoro-3,7-Dimethyl-5,10a-Dihydro-1H-5l4,6l4-Dipyrrolo[1,2-c:2′,1′-f][1,3,2]Diazaborinine (2OD-TBDY-Br$_2$): To a solution of 10-(5-octyldodecylthiophen-2-yl)-5,5-difluoro-3,7-dimethyl-5,10a-dihydro-1H-5l4,6l4-dipyrrolo[1,2-c:2″,1′-f][1,3,2]diazaborinine (**2OD-TBDY**) (0.289 g, 0.496 mmol) in dry CH_2Cl_2: DMF (6 mL:6 mL) *N*-bromosuccinimide (0.181 g, 1.02 mmol) in CH_2Cl_2 (3 mL) was added under nitrogen, and the mixture was stirred at ambient temperature for 2 h. The reaction mixture was evaporated to dryness to give a crude product, which was purified by column chromatography on silica gel using CH_2Cl_2:hexanes (1:1) as the eluent. The pure product was obtained as dark red oil (0.33 g, 91% yield). ^{1}H NMR (400 MHz, $CDCl_3$): δ 0.88 (t, 6H, J = 6.0 Hz), 1.27–1.33 (m, 33H), 2.63 (s, 6H), 2.85 (d, 2H, J = 6.4 Hz), 6.90 (d, 1H, J = 3.6 Hz), 7.20 (s, 2H), 7.30 (d, 1H, J = 3.6 Hz). ^{13}C NMR (100 MHz, $CDCl_3$): 13.4, 14.1, 22.7, 26.6, 29.3, 29.4, 29.6, 29.7, 29.8, 29.9, 31.8, 31.9, 33.3, 34.8, 40.1, 108.6, 126.7, 130.3, 131.4, 132.3, 132.9, 135.2, 152.1, 154.9. MS(MALDI-TOF) *m/z* (M^+): calcd. for $C_{35}H_{51}BBr_2F_2N_2S$: 738.22, found: 738.357 $[M]^+$, 720.638 $[M\text{-}F]^+$. Anal. calcd. for $C_{35}H_{53}BF_2N_2S$: C, 56.77; H, 6.94; N, 3.78, found: C, 56.97; H, 6.85; N, 3.85.

Synthesis of P(2OD-TBDY-T): A mixture of **2OD-TBDY-Br$_2$** (0.23 g, 0.310 mmol, 1.0 equiv.), 2,5-bis(trimethylstannyl)thiophene (0.127 g, 0.310 mmol, 1.0 equiv.), $Pd_2(dba)_3$ (14.22 mg, 0.016 mmol, 0.05 equiv.), and P(*o*-tolyl)$_3$ (37.8 mg, 0.124 mmol, 0.4 equiv.) in anhydrous toluene (25 mL) was heated at 120 °C for 16 h in a sealed flask under nitrogen. Then, the polymerization mixture was cooled to room temperature, and the viscous mixture was poured into methanol (≈200 mL). After stirring for 1h, the precipitated dark solid was collected by gravity filtration. The crude polymer solid was subjected to sequential Soxhlet extractions with methanol, acetone, hexanes, and chloroform. Finally, the concentrated chloroform solution (≈10 mL) was precipitated into methanol (≈200 mL). The extraction/precipitation procedure was repeated three times in total. The final precipitate was collected by vacuum filtration and dried under reduced pressure to give the pure polymer as a dark-colored solid (186 mg, 91% yield). Elemental analysis calcd. for $C_{39}H_{53}BF_2N_2S_2$: C, 70.67; H, 8.06; N, 4.23; found: C, 70.86; H, 8.15; N, 4.55; GPC (RT in THF): M_n = 75.3 kDa, M_w = 398.6 kDa, and PDI = 5.29 (against PS standard).

Synthesis of P(2OD-TBDY-TT): A mixture of **2OD-TBDY-Br$_2$** (0.44 g, 0.59 mmol, 1.0 equiv.), 2,5-bis(trimethylstannyl)thieno[3,2-b]thiophene (0.285 g, 0.59 mmol, 1.0 equiv.), $Pd_2(dba)_3$ (20.72 mg, 29 µmol, 0.05 equiv.), and P(*o*-tolyl)$_3$ (72.3 mg, 237.6 µmol, 0.4 equiv.) in anhydrous toluene (50 mL) was heated at 120 °C for 5 min in a sealed flask under nitrogen. Then, the polymerization mixture was cooled to room temperature, and the viscous mixture was poured into methanol (≈750 mL). After stirring for 1h, the precipitated dark solid was collected by gravity filtration. The crude polymer solid was subjected to sequential Soxhlet extractions with methanol, acetone, hexanes, and chloroform. Finally, the concentrated chloroform solution (≈100 mL) was precipitated into methanol (≈2000 mL). The extraction/precipitation procedure was repeated three times in total. The final precipitate was collected by vacuum filtration and dried under reduced pressure to give the pure polymer as a dark-colored solid (85 mg, 20% yield). Elemental analysis calcd. for $C_{41}H_{53}BF_2N_2S_3$: C, 68.50; H, 7.43; N, 3.90; found: C, 68.78; H, 7.85; N, 3.65; GPC (RT in THF): M_n = 11.0 kDa, M_w = 112.0 kDa, and PDI = 10.21 (against PS standard).

Fabrication and Characterization of OFET Devices: All OFETs were fabricated on highly n-doped silicon wafers having thermally oxidized 300 nm SiO_2 dielectric (capacitance per unit area, C_i = 11.4 nF cm^{-2}) by adopting the top-contact/bottom-gate device architecture. The substrates were cleaned via sonication in acetone for 10 min followed by oxygen plasma cleaning for 5 min (Harrick plasma, PDC-32G, 18 W). The PS (polystyrene)-brush treatment was performed in accordance with the reported procedures (M_w = 1.7–10 kg mol^{-1}) to achieve favorable dielectric–semiconductor interfaces.[75] The polymeric semiconductor films (**P(2OD-TBDY-T)** and **P(2OD-TBDY-TT)**) were deposited via spin coating (≈5–7 mg mL^{-1} in chloroform) on PS-brush-treated substrates, followed by thermal annealing at 70 °C to remove residual solvents. The profilometer (DEKTAK-XT, Bruker) was used to measure the polymer film thicknesses (≈50–60 nm). The top electrodes were thermally evaporated (deposition rate = 0.2 Å s^{-1}) as Au layers (50 nm) with various channel widths (W, 1000 and 500 µm) and lengths (L, 100 and 50 µm). Keithley 4200-SCS was used to characterize the electrical performances of OFETs in ambient at room temperature. The electronic performance in the saturation region such as charge-carrier mobilities (μ) and threshold voltages (V_T) was extracted from the equation

$$\mu_{sat} = (2I_{DS}L)/\left[WC_i(V_G - V_T)^2\right] \quad (1)$$

where I_{DS} is the drain current, L and W are the channel length and width, respectively, C_i is the areal capacitance of the gate dielectric, V_G is the gate voltage, and V_T is the threshold voltage. The surface morphology and microstructure of thin films were measured by atomic force microscopy (NX10, Park systems), field-emission scanning electron microscope (FE-SEM, Zeiss EVO LS 10), and XRD (Smartlab, Rigaku).

Fabrication and Characterization of Inverted OPV Devices: The BHJ-OPV devices of inverted type were fabricated with the structure of ITO/ZnO/active layer **(P(2OD-TBDY-T)**:$PC_{71}BM$))/MoO_3/Ag. The patterned ITO substrates were cleaned by ultrasonication in acetone, DI water, and isopropyl alcohol for 20 min at each step. Then, the ITO substrates were dried for 60 min in an oven at 80 °C. The ITO substrates were treated with plasma prior to the spin coating of ZnO solution at 4000 rpm for 40 s and baking for 20 min at 200 °C in ambient air. The devices were transferred to an N_2-filled glovebox. **P(2OD-TBDY-T)**:$PC_{71}BM$ (ratio 1:1.5 w/w) dissolved in chloroform (12 mg mL^{-1}) with or without 3 vol% DIO additive was spin-coated onto the ZnO layer at 3000 rpm for 40 s. 10 nm of MoO_3 layer followed by a Ag layer (120 nm) was thermally evaporated under high vacuum ($<10^{-6}$ Torr). The *J*–*V* characteristics of the devices were measured with a Keithley 2400 SMU under AM 1.5G (100 mW cm^{-2}) solar irradiation (Peccell: PEC-L01). The EQE was obtained using a solar cell spectral response measurement system (K3100 IQX, McScience Inc.) at ambient conditions. A monochromatic light from a xenon arc lamp at 300 W processed by a monochromator (Newport) and an optical chopper (MC 2000 Thorlabs) was used to apply this spectral measurement system. The morphology of the polymer:fullerene blend was studied by AFM (Veeco Dimension 3100) in tapping mode and a TEM (JEM-3011, JEOL).

Supporting Information

Supporting Information is available from the Wiley Online Library or from the author.

Acknowledgements

H.U. acknowledges support from TUBITAK 114M226. C.K. acknowledges support from mid-career researcher program through the National Research Foundation of Korea (NRF) (NRF-2017R1A2B4001955). B.J.K. acknowledges support from the New and Renewable Energy Core Technology Program of the Korea Institute of Energy Technology Evaluation and Planning (KETEP) (20163010012470). M.-G.K. acknowledges support from the National Research Foundation of Korea (NRF) (NRF-2016K2A9A1A06924256).

Conflict of Interest

The authors declare no conflict of interest.

Keywords

BODIPY, donor–acceptor copolymers, field-effect transistors, photovoltaics, semiconducting polymers

Received: July 31, 2017
Revised: September 21, 2017
Published online: December 11, 2017

[1] V. Shrotriya, *Nat. Photonics* **2009**, *3*, 447.
[2] M. Kaltenbrunner, M. S. White, E. D. Głowacki, T. Sekitani, T. Someya, N. S. Sariciftci, S. Bauer, *Nat. Commun.* **2012**, *3*, 770.
[3] T. Kim, J.-H. Kim, T. E. Kang, C. Lee, H. Kang, M. Shin, C. Wang, B. Ma, U. Jeong, T.-S. Kim, B. J. Kim, *Nat. Commun.* **2015**, *6*, 8547.
[4] H. T. Yi, M. M. Payne, J. E. Anthony, V. Podzorov, *Nat. Commun.* **2012**, *3*, 1259.
[5] C.-H. Cho, H. J. Kim, H. Kang, T. J. Shin, B. J. Kim, *J. Mater. Chem.* **2012**, *22*, 14236.
[6] T. E. Kang, H.-H. Cho, C.-H. Cho, K.-H. Kim, H. Kang, M. Lee, S. Lee, B. Kim, C. Im, B. J. Kim, *ACS Appl. Mater. Interfaces* **2013**, *5*, 861.
[7] M.-C. Chen, S. Vegiraju, C.-M. Huang, P.-Y. Huang, K. Prabakaran, S. L. Yau, W.-C. Chen, W.-T. Peng, I. Chao, C. Kim, Y.-T. Tao, *J. Mater. Chem. C* **2014**, *2*, 8892.
[8] S. S. Cheng, P. Y. Huang, M. Ramesh, H. C. Chang, L. M. Chen, C. M. Yeh, C. L. Fung, M. C. Wu, C. C. Liu, C. Kim, H. C. Lin, M. C. Chen, C. W. Chu, *Adv. Funct. Mater.* **2014**, *24*, 2057.
[9] L. Zhang, N. S. Colella, B. P. Cherniawski, S. C. B. Mannsfeld, A. L. Briseno, *ACS Appl. Mater. Interfaces* **2014**, *6*, 5327.
[10] V. Figà, C. Chiappara, F. Ferrante, M. P. Casaletto, F. Principato, S. Cataldo, Z. Chen, H. Usta, A. Facchetti, B. Pignataro, *J. Mater. Chem. C* **2015**, *3*, 5985.
[11] A. Facchetti, *Chem. Mater.* **2011**, *23*, 733.
[12] S. Fabiano, H. Usta, R. Forchheimer, X. Crispin, A. Facchetti, M. Berggren, *Adv. Mater.* **2014**, *26*, 7438.
[13] A. Marrocchi, A. Facchetti, D. Lanari, S. Santoro, L. Vaccaro, *Chem. Sci.* **2016**, *7*, 6298.
[14] F. Silvestri, A. Marrocchi, M. Seri, C. Kim, T. J. Marks, A. Facchetti, A. Taticchi, *J. Am. Chem. Soc.* **2010**, *132*, 6108.
[15] L. Zhang, A. Fonari, Y. Liu, A.-L. M. Hoyt, H. Lee, D. Granger, S. Parkin, T. P. Russell, J. E. Anthony, J.-L. Brédas, V. Coropceanu, A. L. Briseno, *J. Am. Chem. Soc.* **2014**, *136*, 9248.
[16] C. Grand, S. Baek, T.-H. Lai, N. Deb, W. Zajaczkowski, R. Stalder, K. Müllen, W. Pisula, D. G. Bucknall, F. So, J. R. Reynolds, *Macromolecules* **2016**, *49*, 4008.
[17] T. Lei, Y. Cao, Y. Fan, C.-J. Liu, S.-C. Yuan, J. Pei, *J. Am. Chem. Soc.* **2011**, *133*, 6099.
[18] I. Meager, M. Nikolka, B. C. Schroeder, C. B. Nielsen, M. Planells, H. Bronstein, J. W. Rumer, D. I. James, R. S. Ashraf, A. Sadhanala, P. Hayoz, J. C. Flores, H. Sirringhaus, I. McCulloch, *Adv. Funct. Mater.* **2014**, *24*, 7109.
[19] Y.-J. Cheng, S.-H. Yang, C.-S. Hsu, *Chem. Rev.* **2009**, *109*, 5868.
[20] H. Zhou, L. Yang, W. You, *Macromolecules* **2012**, *45*, 607.
[21] Y. Liang, D. Feng, Y. Wu, S.-T. Tsai, G. Li, C. Ray, L. Yu, *J. Am. Chem. Soc.* **2009**, *131*, 7792.
[22] V. Vohra, K. Kawashima, T. Kakara, T. Koganezawa, I. Osaka, K. Takimiya, H. Murata, *Nat. Photonics* **2015**, *9*, 403.
[23] Z. He, C. Zhong, S. Su, M. Xu, H. Wu, Y. Cao, *Nat. Photonics* **2012**, *6*, 593.
[24] Y. Liu, J. Zhao, Z. Li, C. Mu, W. Ma, H. Hu, K. Jiang, H. Lin, H. Ade, H. Yan, *Nat. Commun.* **2014**, *5*, 5293.
[25] H. Hu, K. Jiang, G. Yang, J. Liu, Z. Li, H. Lin, Y. Liu, J. Zhao, J. Zhang, F. Huang, Y. Qu, W. Ma, H. Yan, *J. Am. Chem. Soc.* **2015**, *137*, 14149.
[26] T. E. Kang, K.-H. Kim, B. J. Kim, *J. Mater. Chem. A* **2014**, *2*, 15252.
[27] K.-H. Kim, S. Park, H. Yu, H. Kang, I. Song, J. H. Oh, B. J. Kim, *Chem. Mater.* **2014**, *26*, 6963.
[28] Y. Lin, X. Zhan, *Acc. Chem. Res.* **2016**, *49*, 175.
[29] W. Zhao, S. Li, H. Yao, S. Zhang, Y. Zhang, B. Yang, J. Hou, *J. Am. Chem. Soc.* **2017**, *139*, 7148.
[30] W. Zhao, D. Qian, S. Zhang, S. Li, O. Inganäs, F. Gao, J. Hou, *Adv. Mater.* **2016**, *28*, 4734.
[31] K. H. Hendriks, G. H. L. Heintges, V. S. Gevaerts, M. M. Wienk, R. A. J. Janssen, *Angew. Chem., Int. Ed.* **2013**, *52*, 8341.

[32] H. Bronstein, Z. Chen, R. S. Ashraf, W. Zhang, J. Du, J. R. Durrant, P. Shakya Tuladhar, K. Song, S. E. Watkins, Y. Geerts, M. M. Wienk, R. A. J. Janssen, T. Anthopoulos, H. Sirringhaus, M. Heeney, I. McCulloch, *J. Am. Chem. Soc.* **2011**, *133*, 3272.
[33] E. Wang, Z. Ma, Z. Zhang, K. Vandewal, P. Henriksson, O. Inganäs, F. Zhang, M. R. Andersson, *J. Am. Chem. Soc.* **2011**, *133*, 14244.
[34] K. Kranthiraja, K. Gunasekar, H. Kim, A.-N. Cho, N.-G. Park, S. Kim, B. J. Kim, R. Nishikubo, A. Saeki, M. Song, S.-H. Jin, *Adv. Mater.* **2017**, *29*, 1700183.
[35] N. Zhou, A. S. Dudnik, T. I. N. G. Li, E. F. Manley, T. J. Aldrich, P. Guo, H.-C. Liao, Z. Chen, L. X. Chen, R. P. H. Chang, A. Facchetti, M. Olvera de la Cruz, T. J. Marks, *J. Am. Chem. Soc.* **2016**, *138*, 1240.
[36] X. Zhan, Z. Tan, B. Domercq, Z. An, X. Zhang, S. Barlow, Y. Li, D. Zhu, B. Kippelen, S. R. Marder, *J. Am. Chem. Soc.* **2007**, *129*, 7246.
[37] H. Usta, C. Newman, Z. Chen, A. Facchetti, *Adv. Mater.* **2012**, *24*, 3678.
[38] Z. Chen, Y. Zheng, H. Yan, A. Facchetti, *J. Am. Chem. Soc.* **2009**, *131*, 8.
[39] E. Zhou, J. Cong, Q. Wei, K. Tajima, C. Yang, K. Hashimoto, *Angew. Chem., Int. Ed.* **2011**, *50*, 2799.
[40] C. Lee, H. Kang, W. Lee, T. Kim, K.-H. Kim, H. Y. Woo, C. Wang, B. J. Kim, *Adv. Mater.* **2015**, *27*, 2466.
[41] M. Ozdemir, D. Choi, G. Kwon, Y. Zorlu, B. Cosut, H. Kim, A. Facchetti, C. Kim, H. Usta, *ACS Appl. Mater. Interfaces* **2016**, *8*, 14077.
[42] L. Huang, Z. Li, Y. Zhao, Y. Zhang, S. Wu, J. Zhao, G. Han, *J. Am. Chem. Soc.* **2016**, *138*, 14586.
[43] C. L. Teoh, D. Su, S. Sahu, S.-W. Yun, E. Drummond, F. Prelli, S. Lim, S. Cho, S. Ham, T. Wisniewski, Y.-T. Chang, *J. Am. Chem. Soc.* **2015**, *137*, 13503.
[44] K. Tanaka, Y. Chujo, *Macromol. Rapid Commun.* **2012**, *33*, 1235.
[45] A. Nagai, J. Miyake, K. Kokado, Y. Nagata, Y. Chujo, *J. Am. Chem. Soc.* **2008**, *130*, 15276.
[46] T. Bura, N. Leclerc, S. Fall, P. Lévêque, T. Heiser, P. Retailleau, S. Rihn, A. Mirloup, R. Ziessel, *J. Am. Chem. Soc.* **2012**, *134*, 17404.
[47] B. M. Squeo, N. Gasparini, T. Ameri, A. Palma-Cando, S. Allard, V. G. Gregoriou, C. J. Brabec, U. Scherf, C. L. Chochos, *J. Mater. Chem. A* **2015**, *3*, 16279.
[48] F. Li, Y. Chen, C. Ma, U. Buttner, K. Leo, T. Wu, *Adv. Electron. Mater.* **2017**, *3*, 1600430.
[49] H. Usta, M. D. Yilmaz, A.-J. Avestro, D. Boudinet, M. Denti, W. Zhao, J. F. Stoddart, A. Facchetti, *Adv. Mater.* **2013**, *25*, 4327.
[50] I. Bulut, Q. Huaulmé, A. Mirloup, P. Chávez, S. Fall, A. Hébraud, S. Méry, B. Heinrich, T. Heiser, P. Lévêque, N. Leclerc, *ChemSusChem* **2017**, *10*, 1878.
[51] V. Leen, P. Yuan, L. Wang, N. Boens, W. Dehaen, *Org. Lett.* **2012**, *14*, 6150.
[52] Y. Hayashi, S. Yamaguchi, W. Y. Cha, D. Kim, H. Shinokubo, *Org. Lett.* **2011**, *13*, 2992.
[53] A. Poirel, A. De Nicola, P. Retailleau, R. Ziessel, *J. Org. Chem.* **2012**, *77*, 7512.
[54] L. Jiao, W. Pang, J. Zhou, Y. Wei, X. Mu, G. Bai, E. Hao, *J. Org. Chem.* **2011**, *76*, 9988.
[55] A. B. Nepomnyashchii, M. Bröring, J. Ahrens, A. J. Bard, *J. Am. Chem. Soc.* **2011**, *133*, 8633.
[56] B. M. Squeo, V. G. Gregoriou, A. Avgeropoulos, S. Baysec, S. Allard, U. Scherf, C. L. Chochos, *Prog. Polym. Sci.* **2017**, *71*, 26.
[57] T. Bura, N. Leclerc, S. Fall, P. Lévêque, T. Heiser, P. Retailleau, S. Rihn, A. Mirloup, R. Ziessel, *J. Am. Chem. Soc.* **2012**, *134*, 17404.
[58] A. M. Poe, A. M. Della Pelle, A. V. Subrahmanyam, W. White, G. Wantz, S. Thayumanavan, *Chem. Commun.* **2014**, *50*, 2913.
[59] D. Cortizo-Lacalle, C. T. Howells, S. Gambino, F. Vilela, Z. Vobecka, N. J. Findlay, A. R. Inigo, S. A. J. Thomson, P. J. Skabara, I. D. W. Samuel, *J. Mater. Chem.* **2012**, *22*, 14119.
[60] B. Kim, B. Ma, V. R. Donuru, H. Liu, J. M. J. Fréchet, *Chem. Commun.* **2010**, *46*, 4148.
[61] W. He, Y. Jiang, Y. Qin, *Polym. Chem.* **2014**, *5*, 1298.
[62] Z. Xu, L.-M. Chen, G. Yang, C.-H. Huang, J. Hou, Y. Wu, G. Li, C.-S. Hsu, Y. Yang, *Adv. Funct. Mater.* **2009**, *19*, 1227.
[63] M. Ozdemir, D. Choi, Y. Zorlu, B. Cosut, H. Kim, C. Kim, H. Usta, *New J. Chem.* **2017**, *41*, 6232.
[64] J. A. Letizia, M. R. Salata, C. M. Tribout, A. Facchetti, M. A. Ratner, T. J. Marks, *J. Am. Chem. Soc.* **2008**, *130*, 9679.
[65] B. Carsten, J. M. Szarko, L. Lu, H. J. Son, F. He, Y. Y. Botros, L. X. Chen, L. Yu, *Macromolecules* **2012**, *45*, 6390.
[66] T. Lei, J.-H. Dou, J. Pei, *Adv. Mater.* **2012**, *24*, 6457.
[67] H. Hu, K. Jiang, J.-H. Kim, G. Yang, Z. Li, T. Ma, G. Lu, Y. Qu, H. Ade, H. Yan, *J. Mater. Chem. A* **2016**, *4*, 5039.
[68] S. Shi, J. Yuan, G. Ding, M. Ford, K. Lu, G. Shi, J. Sun, X. Ling, Y. Li, W. Ma, *Adv. Funct. Mater.* **2016**, *26*, 5669.
[69] S. Lu, M. Drees, Y. Yao, D. Boudinet, H. Yan, H. Pan, J. Wang, Y. Li, H. Usta, A. Facchetti, *Macromolecules* **2013**, *46*, 3895.
[70] H. Hu, K. Jiang, J.-H. Kim, G. Yang, Z. Li, T. Ma, G. Lu, Y. Qu, H. Ade, H. Yan, *J. Mater. Chem. A* **2016**, *4*, 5039.
[71] X. Long, Z. Ding, C. Dou, J. Zhang, J. Liu, L. Wang, *Adv. Mater.* **2016**, *28*, 6504.
[72] A. Zitzler-Kunkel, M. R. Lenze, K. Meerholz, F. Würthner, *Chem. Sci.* **2013**, *4*, 2071.
[73] H. Kar, S. Ghosh, *Chem. Commun.* **2016**, *52*, 8818.
[74] M. Yilmaz, M. Erkartal, M. Ozdemir, U. Sen, H. Usta, G. Demirel, *ACS Appl. Mater. Interfaces* **2017**, *9*, 18199.
[75] S. H. Park, H. S. Lee, J.-D. Kim, D. W. Breiby, E. Kim, Y. D. Park, D. Y. Ryu, D. R. Lee, J. H. Cho, *J. Mater. Chem.* **2011**, *21*, 15580.
[76] J. Y. Na, B. Kang, D. H. Sin, K. Cho, Y. D. Park, *Sci. Rep.* **2015**, *5*, 13288.
[77] X. Guo, N. Zhou, S. J. Lou, J. W. Hennek, R. Ponce Ortiz, M. R. Butler, P. T. Boudreault, J. Strzalka, P. Morin, M. Leclerc, J. T. López Navarrete, M. A. Ratner, L. X. Chen, R. P. H. Chang, A. Facchetti, T. J. Marks, *J. Am. Chem. Soc.* **2012**, *134*, 18427.
[78] S. G. J. Mathijssen, M. Cölle, H. Gomes, E. C. P. Smits, B. de Boer, I. McCulloch, P. A. Bobbert, D. M. de Leeuw, *Adv. Mater.* **2007**, *19*, 2785.
[79] H. Yan, Z. Chen, Y. Zheng, C. Newman, J. R. Quinn, F. Dötz, M. Kastler, A. Facchetti, *Nature* **2009**, *457*, 679.
[80] R. J. Kline, M. D. McGehee, E. N. Kadnikova, J. Liu, J. M. J. Frechet, M. F. Toney, *Macromolecules* **2005**, *38*, 3312.
[81] M. Ozdemir, D. Choi, G. Kwon, Y. Zorlu, H. Kim, M.-G. Kim, S. Seo, U. Sen, M. Citir, C. Kim, H. Usta, *RSC Adv.* **2016**, *6*, 212.
[82] R. P. Ortiz, H. Herrera, C. Seoane, J. L. Segura, A. Facchetti, T. J. Marks, *Chem. – Eur. J.* **2012**, *18*, 532.
[83] H. Sirringhaus, P. J. Brown, R. H. Friend, M. M. Nielsen, K. Bechgaard, B. M. W. Langeveld-Voss, A. J. H. Spiering, R. A. J. Janssen, E. W. Meijer, P. Herwig, D. M. de Leeuw, *Nature* **1999**, *401*, 685.
[84] S. K. Hau, H.-L. Yip, A. K.-Y. Jen, *Polym. Rev.* **2010**, *50*, 474.
[85] K.-H. Kim, H. Kang, H. J. Kim, P. S. Kim, S. C. Yoon, B. J. Kim, *Chem. Mater.* **2012**, *24*, 2373.
[86] D. J. Kang, H. Kang, K.-H. Kim, B. J. Kim, *ACS Nano* **2012**, *6*, 7902.
[87] H. Kang, M. A. Uddin, C. Lee, K.-H. Kim, T. L. Nguyen, W. Lee, Y. Li, C. Wang, H. Y. Woo, B. J. Kim, *J. Am. Chem. Soc.* **2015**, *137*, 2359.
[88] K. Gao, J. Miao, L. Xiao, W. Deng, Y. Kan, T. Liang, C. Wang, F. Huang, J. Peng, Y. Cao, F. Liu, T. P. Russell, H. Wu, X. Peng, *Adv. Mater.* **2016**, *28*, 4727.
[89] J. Chen, L. Zhang, X. Jiang, K. Gao, F. Liu, X. Gong, J. Chen, Y. Cao, *Adv. Energy Mater.* **2017**, *7*, 1601344.

[90] D. H. Wang, P.-O. Morin, C.-L. Lee, A. K. Ko Kyaw, M. Leclerc, A. J. Heeger, *J. Mater. Chem. A* **2014**, *2*, 15052.
[91] G. Zhang, Y. Fu, Q. Zhang, Z. Xie, *Chem. Commun.* **2010**, *46*, 4997.
[92] L. Huo, T. Liu, X. Sun, Y. Cai, A. J. Heeger, Y. Sun, *Adv. Mater.* **2015**, *27*, 2938.
[93] H. Qin, L. Li, F. Guo, S. Su, J. Peng, Y. Cao, X. Peng, *Energy Environ. Sci.* **2014**, *7*, 1397.
[94] G. Ren, E. Ahmed, S. A. Jenekhe, *Adv. Energy Mater.* **2011**, *1*, 946.
[95] P. Cheng, L. Ye, X. Zhao, J. Hou, Y. Li, X. Zhan, *Energy Environ. Sci.* **2014**, *7*, 1351.
[96] J. Peet, J. Y. Kim, N. E. Coates, W. L. Ma, D. Moses, A. J. Heeger, G. C. Bazan, *Nat. Mater.* **2007**, *6*, 497.
[97] Z. Li, X. Xu, W. Zhang, X. Meng, W. Ma, A. Yartsev, O. Inganäs, M. R. Andersson, R. A. J. Janssen, E. Wang, *J. Am. Chem. Soc.* **2016**, *138*, 10935.
[98] G. Li, R. Zhu, Y. Yang, *Nat. Photonics* **2012**, *6*, 153.
[99] S. Mukherjee, C. M. Proctor, J. R. Tumbleston, G. C. Bazan, T.-Q. Nguyen, H. Ade, *Adv. Mater.* **2015**, *27*, 1105.
[100] W. Ma, J. R. Tumbleston, M. Wang, E. Gann, F. Huang, H. Ade, *Adv. Energy Mater.* **2013**, *3*, 864.
[101] M. J. Frisch, G. W. Trucks, H. B. Schlegel, G. E. Scuseria, M. A. Robb, J. R. Cheeseman, G. Scalmani, V. Barone, B. Mennucci, G. A. Petersson, H. Nakatsuji, M. Caricato, X. Li, H. P. Hratchian, A. F. Izmaylov, J. Bloino, G. Zheng, J. L. Sonnenberg, M. Hada, M. Ehara, K. Toyota, R. Fukuda, J. Hasegawa, M. Ishida, T. Nakajima, Y. Honda, O. Kitao, H. Nakai, T. Vreven, J. A. Montgomery Jr., J. E. Peralta, F. Ogliaro, M. Bearpark, J. J. Heyd, E. Brothers, K. N. Kudin, V. N. Staroverov, T. Keith, R. Kobayashi, J. Normand, K. Raghavachari, A. Rendell, J. C. Burant, S. S. Iyengar, J. Tomasi, M. Cossi, N. Rega, J. M. Millam, M. Klene, J. E. Knox, J. B. Cross, V. Bakken, C. Adamo, J. Jaramillo, R. Gomperts, R. E. Stratmann, O. Yazyev, A. J. Austin, R. Cammi, C. Pomelli, J. W. Ochterski, R. L. Martin, K. Morokuma, V. G. Zakrzewski, G. A. Voth, P. Salvador, J. J. Dannenberg, S. Dapprich, A. D. Daniels, O. Farkas, J. B. Foresman, J. V. Ortiz, J. Cioslowski, D. J. Fox, *Gaussian 09, Revision C.01*, Gaussian, Inc., Wallingford CT **2010**.
[102] S. Subramaniyan, H. Xin, F. S. Kim, S. A. Jenekhe, *Macromolecules* **2011**, *44*, 6245.

